Journal of Hazardous Materials 403 (2021) 123912

Contents lists available at ScienceDirect

Journal of Hazardous Materials

journal homepage: www.elsevier.com/locate/jhazmat

Arsenic detoxification by iron-manganese nodules under electrochemically controlled redox: Mechanism and application

Lihu Liu [a], Qi Qiao [a], Wenfeng Tan [a], Xuecheng Sun [a], Chengshuai Liu [b], Zhi Dang [c], Guohong Qiu [a,*]

[a] Key Laboratory of Arable Land Conservation (Middle and Lower Reaches of Yangtse River), Ministry of Agriculture and Rural Affairs, Hubei Key Laboratory of Soil Environment and Pollution Remediation, College of Resources and Environment, Interdisciplinary Sciences Research Institute, Huazhong Agricultural University, Wuhan, 430070, Hubei Province, China

[b] State Key Laboratory of Environmental Geochemistry, Institute of Geochemistry, Chinese Academy of Sciences, Guiyang, 550081, Guizhou Province, China

[c] School of Environment and Energy, South China University of Technology, Guangzhou, 510006, Guangdong Province, China

ARTICLE INFO

Editor: Danmeng Shuai

Keywords:
Iron-manganese nodule
Arsenic
Electrochemical adsorption
Symmetric electrode
Redox

ABSTRACT

Iron-manganese binary oxides are characterized by high oxidation and adsorption capability and widely applied to arsenic (As) detoxification in contaminated waters. Despite of their lower preparation cost relative to synthesized iron-manganese binary oxides, the low adsorption capacity of natural iron-manganese oxides largely hinders their application. Here, electrochemically controlled redox was employed to improve the As(III,V) removal performance of iron-manganese nodules in a symmetric electrode system, and the removal mechanism and electrode reusability were also examined. Experimental results showed that both the electrochemical reduction and oxidation of birnessite in iron-manganese nodules contributed much to As(III,V) removal. Higher cell voltage facilitated a higher removal efficiency of total As within 0–1.2 V, which reached 94.7% at 1.2 V for actual As-containing wastewater (4068 μg L^{-1}). The efficiency was obviously higher than that at open circuit (81.4%). Under electrode polarity reversal, the alternating reduction dissolution and oxidation recrystallization of birnessite in iron-manganese nodules promoted their contact with As, enhancing the total As removal efficiency from 75.6% to 91.8% after five times of repeated adsorption. This research clarifies the effect of electrochemical redox on As(III,V) detoxification by iron-manganese oxides, and expands the application of natural iron-manganese nodules in the treatment of As-contaminated wastewaters.

1. Introduction

Metalloid arsenic (As) has high toxic and carcinogenic properties (Ociński et al., 2016). The maximum permissible As concentration in drinking water is 10 μg L^{-1} (World Health Organization standard) due to its health and environmental risks (Ociński et al., 2016). Inorganic As is mainly present as As(III) and As(V) in natural waters, with the former being dozens of times more toxic than the latter (Shan and Tong, 2013). In oxidizing environments, As exists primarily as $H_2AsO_4^-$ and $HAsO_4^{2-}$ with a weak acid or weak alkaline pH value; while in reducing environments, As is present mostly as uncharged H_3AsO_3 with pH < 9 (Dai et al., 2018). Therefore, As(III) is more difficult to be removed than As (V).

As an easy-operation, low-cost and high-selectivity method, adsorption has been extensively investigated and used for As detoxification of contaminated waters (Alvarez-Cruz and Garrido-Hoyos, 2019; Wei et al., 2019). Manganese oxides can easily oxidize As(III) to As(V) (Gude et al., 2017); and iron oxides show strong affinity for As(V) due to their high point of zero charge (5.5–9.0) and abundant surface hydroxyl groups (Eljamal et al., 2018; Luong et al., 2018). Iron-manganese binary oxides have both the oxidation characteristics of manganese oxides and the adsorption capability of iron oxides, which synergistically contribute to a higher As(III) removal efficiency than single manganese oxides or iron oxides (Shan and Tong, 2013; Zheng et al., 2020). Therefore, iron-manganese binary oxides are widely used in the purification of As-containing wastewaters (Bai et al., 2016; Gude et al., 2017; Zheng et al., 2020). Currently, iron-manganese binary oxides are mostly obtained by biotic or chemical synthesis methods, which involve multi-step operation or high cost (Bai et al., 2016; Zheng et al., 2020). There are abundant resources of iron and

* Corresponding author.
E-mail address: qiugh@mail.hzau.edu.cn (G. Qiu).

https://doi.org/10.1016/j.jhazmat.2020.123912
Received 31 July 2020; Received in revised form 5 September 2020; Accepted 7 September 2020
Available online 14 September 2020

manganese oxide minerals in natural environments (Ying et al., 2012). However, their adsorption and oxidation capacities are far lower than those of the synthesized iron-manganese binary oxides due to the coexisting impurities such as quartz (Gasparatos, 2013). Therefore, enhancement of the adsorption and oxidation capacity of easily available natural iron-manganese oxides facilitates the reduction of the preparation cost and practical application in the treatment of As-containing wastewaters.

Iron and manganese oxides often co-exist as nodules in soils and sediments, which also contain some primary minerals including quartz, feldspar and mica as well as some clay minerals and secondary minerals (Gasparatos, 2013). The abundant iron and manganese oxides in iron-manganese nodules contribute greatly to their As oxidation and adsorption capacity (Zhang et al., 2014). The oxidation and adsorption properties of iron and manganese oxides are directly determined by their crystal structures and chemical compositions (Alvarez-Cruz and Garrido-Hoyos, 2019), which vary greatly under different redox conditions accompanied by the adsorption and desorption of heavy metals. The oxidation of some Fe-containing minerals accelerates the adsorption of anions. For example, the As removal capacity of siderite ($FeCO_3$) in the presence of oxygen could be about 11 folds that under anoxic conditions due to its oxidation transformation to goethite (α-FeOOH) with excellent adsorption performance (Guo et al., 2013). In addition, the reduction of some manganese oxides facilitates their adsorption for heavy metal cations. For instance, the removal capacity of birnessite for Ni^{2+} and Zn^{2+} could be significantly enhanced by its reduction to hausmannite (Mn_3O_4), feitknechtite (β-MnOOH) or hetaerolite ($ZnMn_2O_4$) induced by Mn^{2+} (Lefkowitz and Elzinga, 2017; Zhao et al., 2018). Therefore, it can be speculated that the As(III) oxidation and As (V) adsorption performance of natural iron-manganese nodules can be improved by adjusting the redox reactions with changes in the crystal structure and chemical composition of iron and manganese oxides.

The redox reactions of iron and manganese oxides can be accurately controlled by using electrochemical techniques (Liu et al., 2016). In our previous work, the electrochemical reduction of manganese oxides was found to contribute greatly to their adsorption for heavy metal ions including Cu^{2+}, Cd^{2+} and Zn^{2+} because of the changes in chemical composition, crystal structure and surface charge (Liu et al., 2017, 2018; Yang et al., 2018; Liu et al., 2019a). The total As removal efficiency of iron-manganese nodule anode increased from 70.5% to 83.6% at 1.2 V cell voltage in an asymmetric electrode system using a carbon fiber as the cathode, which was ascribed to the increase in positive charges on iron-manganese nodule surface (Qiao et al., 2020). The interaction between As(III,V) and iron-manganese nodules under electrochemical reduction is different from that under electrochemical oxidation. Fe^{2+} may be released during iron oxide reduction and participate in the Fenton reaction with H_2O_2 formed through the electrochemical reduction of O_2, promoting the oxidation of As(III) (Liu et al., 2019b); and the reduction of $Mn(IV)O_6$ to $Mn(III)O_6$ can provide more adsorption sites for As(V) at the edge of MnO_6 octahedral layer (Lafferty et al., 2010). The released cations of Fe^{2+} and Mn^{2+} from the reduction of iron-manganese nodule cathode may be re-oxidized on the anode. Moreover, some cations including Ca^{2+} and Mg^{2+} can complex or precipitate with As(III,V) (Chille et al., 2018), which will affect As oxidation and adsorption in actual waters. The adsorption mechanism of iron-manganese nodules for As(III,V) and the influencing factors remain largely unknown at the co-existence of electrochemical oxidation and reduction.

Reusability is also an important index to evaluate the application value of adsorbents. Although the adsorption in the form of inner-sphere complexes for As on iron and manganese oxides can greatly increase the removal capacity (Zhang et al., 2014), it may also hinder the desorption of As and the reuse of adsorbents. It remains challenging to further improve the adsorption and reusability of iron-manganese nodules. In this work, a symmetric iron-manganese nodule electrode system was constructed for As(III,V) removal from actual wastewaters. The coexisting electrochemical oxidation and reduction were adjusted through cell voltage to study the As removal mechanism and reusability of iron-manganese nodule anode and cathode.

2. Methods

2.1. Sample collection and pretreatment

Iron-manganese nodules were collected from Zaoyang city (E 112°31′38.5″, N 32°16′55.7″), Hubei Province, China, and then dried at 40 °C after rinsing with pure water and alcohol. Fig. S1 shows the photo and FESEM (Field emission scanning electron microscope) image of the collected iron-manganese nodules. A lamellar micromorphology could be observed from the FESEM image. The XRD pattern indicated that the dominant iron and manganese oxides were lithiophorite, birnessite and goethite (Fig. S2). Table S1 presents the contents of some heavy metals including iron and manganese in the collected iron-manganese nodules. The content of iron oxides was calculated to be 222.1 g kg^{-1} using the molecular formula of FeOOH, and that of manganese oxides was determined to be 95.5 g kg^{-1} using the molecular formula of MnO_2, respectively. These data had slight differences from those reported in our previous work, which might be ascribed to the different batches of sampling for these iron-manganese nodules (Qiao et al., 2020).

The As-contaminated water was collected around a metal smelter (E 114°55′47″, N 30°10′18″) in Daye city, Hubei Province, China, which was also used in our previous work (Qiao et al., 2020). The concentrations of As(III) and total As reached 458.8 and 4068.2 μg L^{-1}, respectively, and those of some other ions in the contaminated water are listed in Table S2. The initial pH was detected to be 7.8.

2.2. Electrochemical adsorption of As

Iron-manganese nodule powder, acetylene black and PVDF (polyvinylidene fluoride) were mixed and coated on a graphite paper to prepare the iron-manganese nodule electrode, and the detailed preparation processes are shown in the Supporting Information. The electrochemical adsorption of As by symmetric electrodes (iron-manganese nodule and blank graphite paper electrodes) from 30 mL of contaminated water was performed at different constant cell voltages (0–1.2 V) for 24 h at 25 °C in air atmosphere. Fig. S3 shows the photos of the symmetric electrode system. The adsorption experiments of the synthesized iron-manganese oxide for As at 1.2 V and open circuit were conducted to further investigate the role of iron and manganese oxides. The iron-manganese oxide was prepared through adding 200 mL $FeSO_4$ solution (0.075 mol L^{-1}) to 200 mL $KMnO_4$ solution (0.225 mol L^{-1}) at pH 7–8 (Zhang et al., 2007). The concentration of Ca^{2+} was increased to 300 mg L^{-1} by adding $Ca(NO_3)_2$ to the wastewater to investigate the role of Ca^{2+}. After the electrochemical adsorption, the iron-manganese nodule electrodes were repeatedly used after washing with pure water and dried at 40 °C without any desorption. The effect of electrode polarity reversal on the reusability was examined at 1.2 V. The electrodes were repeatedly used for five times. A Neware CT-3008W-5V1A battery tester was used to control the electrochemical experiments.

2.3. Sample and intermediate characterization

The phase structures of minerals in the iron-manganese nodules were investigated on a Bruker D8 Advance X-ray diffractometer (XRD). The micromorphology and corresponding elemental distribution on the sample surface were analyzed by FESEM/EDX (Hitachi, SU8000). A Multilab 2000 X-ray photoelectron spectrometer (XPS, Mg Kα) with energy calibrated by C 1s peak (284.6 eV) was employed to estimate the elemental valence and relative proportion on the surface of iron-manganese nodules. The clay in iron-manganese nodules was obtained through a siphon method based on the Stokes' law (Roychand and Marschner, 2013). The extracted clay was used as an electrode material

to examine the effect of manganese oxides on electrochemical adsorption, for which the X-ray absorption fine structure (XAFS) spectra were collected at the Beijing Synchrotron Radiation Facility (1W1B beamline), China. More information about the collection and processing of the XAFS data is presented in the Supporting Information. A CEM Mars 6 microwave digester with the mixed solution of HCl and HNO_3 (volume ratio, 3:1) was used for the digestion of iron-manganese nodule powder at 190 °C for 40 min. The concentrations of heavy metal ions in aqueous solution were determined using a Varina AAS240FS atomic adsorption spectrometer. The concentrations of total As and As(III) were analyzed by an Haiguang AFS-9700 atomic fluorescence spectrometer (Xu et al., 2013). The detailed determination method is presented in the Supporting Information. A Mapada UV-1800 ultraviolet-visible spectrophotometer with the wavelength of 551 nm was used to analyze the H_2O_2 concentration by a DPD (*N,N*-diethyl-p-phenylenediamine) method (Garg et al., 2016). The electrode potential was determined using a CHI660E electrochemical workstation (Shanghai Chenhua Instrument Co., Ltd., China) in a three-electrode system with a saturated calomel electrode (SCE) as the reference electrode.

3. Results

3.1. Electrochemical adsorption of As

In the symmetric iron-manganese nodule electrode system, the potential of cathode and anode respectively decreased and increased with the cell voltage rising from 0 to 1.2 V (Fig. S4), and the concentrations of both total As and As(III) decreased (Fig. 1), which were 215.2 and 34.1 μg L^{-1} after electrochemical adsorption at 1.2 V for 24 h, with the corresponding removal efficiency of 94.7% and 92.6%, respectively. The Mn^{2+} concentration was also reduced during As adsorption, which decreased from 4.90 to 4.63 mg L^{-1} at 1.2 V, and reached the minimum of 1.67 mg L^{-1} at 0.3 V (Fig. S5).

The As adsorption by symmetric blank graphite paper electrodes was conducted at 1.2 V and by iron-manganese nodule electrodes at open circuit to comparatively analyze the electrochemical adsorption behaviors of iron-manganese nodules. In these reaction systems, the total As and As(III) concentrations sharply decreased within the first 2 h, followed by slow decreases until reaching a stable status. When iron-manganese nodule electrodes were used, the final total As and As(III) concentrations respectively decreased to 755.1 and 93.5 μg L^{-1}; while when graphite paper electrodes were used instead, they declined to 2264.6 and 192.7 μg L^{-1} (Fig. 2a and b). As shown in the Kim-Yoon plots, the capacity and rate of electrochemical adsorption were higher than those of physicochemical adsorption for the iron-manganese nodules (Fig. 2c). Generally, As is chemically adsorbed on the surface of iron and manganese oxides, forming inner-sphere complexes (Bai et al., 2016; Alvarez-Cruz and Garrido-Hoyos, 2019). The adsorption kinetics of iron-manganese nodule electrodes at 1.2 V and open circuit were fitted using the pseudo-second order model (Fig. 2d and Table S3). The good correlation coefficient also demonstrated the chemical adsorption of As on iron-manganese nodules (Mertens et al., 2012; Dai et al., 2017). The adsorption rate constant at 1.2 V (1.95 g mg^{-1} h^{-1}) was higher than that at open circuit (1.35 g mg^{-1} h^{-1}). These results indicated that this electrochemical technique can be used to enhance the oxidation and adsorption capacities of iron-manganese nodules for As(III,V).

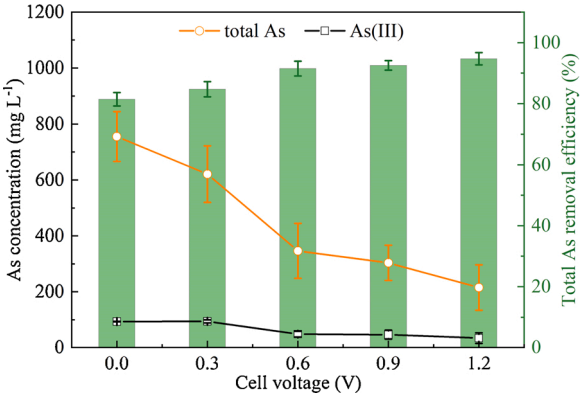

Fig. 1. Arsenic concentration in the wastewater and the corresponding total As removal efficiency after adsorption by symmetric iron-manganese nodule electrodes at different cell voltages for 24 h.

The adsorption of As by the synthesized iron-manganese oxide electrodes was conducted for 24 h to investigate the role of iron and manganese oxides. After electrochemical adsorption at 1.2 V, the total As and As(III) concentrations decreased to 65.5 and 18.0 μg L^{-1}; and at open circuit, they declined to 130.1 and 42.9 μg L^{-1}, respectively. These results indicated that the iron and manganese oxides play important roles in the removal of As.

The chemical compositions, phase structures and micromorphologies of iron-manganese nodules on the anode and cathode were characterized to analyze the electrochemical adsorption process of As. The elemental contents were determined after microwave digestion. The ratios for the content of Fe, Mn and As in the anode to that in the cathode were 1:0.96, 1:1.52, and 1:0.49, respectively, after adsorption at 1.2 V for 24 h. The reduction amount of Mn^{2+} in the wastewater was only about 0.19% of the total amount of Mn in the pristine electrode, indicating that the increased amount of Mn in the anode was mainly derived from the cathode. XRD patterns were then used to characterize the crystal structure of iron-manganese nodules after electrochemical adsorption (Fig. S6). After As adsorption, the XRD patterns of the anode showed no obvious changes; however, the formation of $CaCO_3$ (JCPDS No. 85-1108) was observed on the cathode, and the diffraction intensity increased with increasing cell voltage. The Ca^{2+} concentration also slightly decreased from 152.9 to 151.4 mg L^{-1} after 24 h of electrochemical adsorption in the wastewater. Elemental carbon can be oxidized to CO_2 when the potential is controlled above 0.70 V (*vs.* SHE) (Tang et al., 2017). In this work, the anode potential varied from 0.82 to 1.03 V (*vs.* SHE) at the cell voltage range of 0.6–1.2 V (Fig. S4). Therefore, besides atmospheric CO_2, the electrochemical oxidation of graphite on anode may also lead to the formation of CO_3^{2-} in wastewaters. The FESEM images showed little change in the micromorphology of the electrodes at open circuit and the cathode at 0.6 and 1.2 V, while flower-like crystals were observed on the anode at 0.6 V, which gradually grew and were stacked into spindle-like crystals at 1.2 V (Fig. S7).

3.2. Reusability of iron-manganese nodule electrode

The adsorption capacity of iron-manganese nodules for total As at 1.2 V (0.83 mg g^{-1}) was obviously lower than the physiochemical adsorption capacity (2–5 mg g^{-1}) reported in literature (Chen et al., 2006), indicating that the iron-manganese nodules had not been fully utilized in the electrochemical adsorption. Therefore, the iron-manganese nodule electrodes were repeatedly used in this work without any desorption process. The elemental analysis results indicated that 20.6% of Mn in the cathode was released and re-oxidized on the anode. Hence, the repeated adsorption was conducted with electrode polarity reversal to further improve the utilization ratio of manganese oxides in iron-manganese nodules. Without electrode polarity reversal, the total As removal efficiency gradually decreased from 94.7% to 75.6% after five times of adsorption, with an average removal efficiency of 87.1% (Fig. 3a). With increasing adsorption times, the concentration of Mn^{2+} in the wastewater decreased and reached 0.93 mg L^{-1} at the fifth adsorption (Fig. S8a). When electrode polarity reversal was conducted for each subsequent adsorption, the total As removal efficiency showed little attenuation and was maintained above 90.0%, with an average removal efficiency of 93.3% for the five times of electrochemical adsorption (Fig. 3b). With increasing adsorption times, the concentration of Mn^{2+} in the wastewater firstly increased and reached

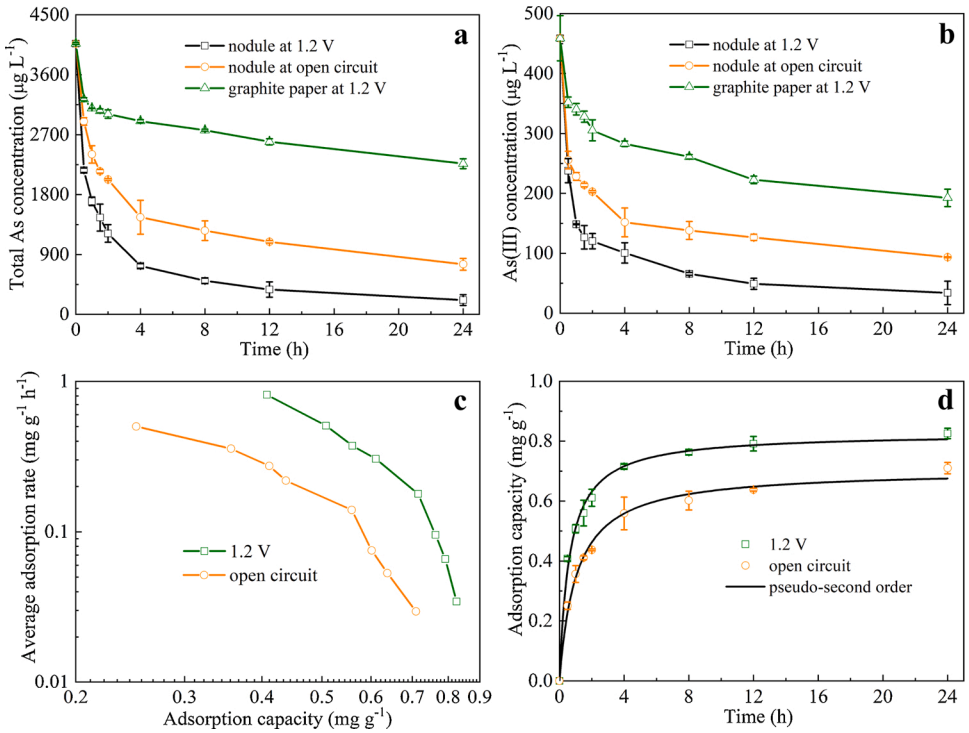

Fig. 2. Total As (a) and As(III) (b) concentrations after adsorption by the symmetric iron-manganese nodule electrodes and by graphite paper electrodes and the corresponding Kim-Yoon plots (c) and total As adsorption kinetics (d) at 1.2 V and open circuit.

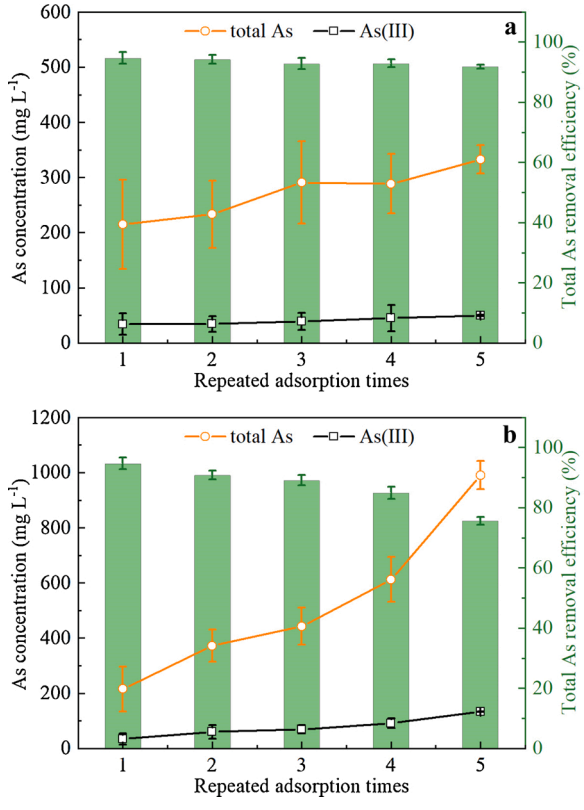

Fig. 3. Arsenic concentration and total As removal efficiency in the wastewater after different times of repeated adsorption by symmetric iron-manganese nodule electrodes without (a) and with (b) electrode polarity reversal at 1.2 V.

the maximum of 5.91 mg L^{-1} at the second adsorption, followed by continuous decreases to 4.11 mg L^{-1} at the fifth adsorption (Fig. S8b). Although some heavy metals co-exist in iron-manganese nodules (Table S1), they were not detected in the wastewater at each adsorption, which may be due to the excellent adsorption performance of iron-manganese nodules (Shan and Tong, 2013; Zheng et al., 2020). These results indicated that no secondary pollution was caused by the toxic heavy metal release during the electrochemical adsorption.

After five times of repeated adsorption, the electrodes were characterized to further analyze the As removal mechanism in view of the low As content in the iron-manganese nodules after the first electrochemical adsorption. The XRD patterns indicated that $CaCO_3$ was generated on the cathodes, and the phase structure of the anodes showed no obvious changes after five times of repeated adsorption with/without electrode polarity reversal (Figs. 4a and S9). Furthermore, the extracted clay was used as the electrode material to examine the effect of manganese oxides on electrochemical adsorption by the linear combination fitting of Mn K-edge EXAFS (extended XAFS) spectra (Fig. 4b). Only the main manganese oxides including lithiophorite and birnessite were selected as the references considering the complex mineral composition of iron-manganese nodules. After five times of repeated adsorption without electrode polarity reversal, the relative proportion of birnessite in the cathode and anode varied from 92.4% to 82.8% and 95.6%, and that of lithiophorite changed from 7.6% to 17.2% and 4.4%, respectively (Table S4), indicating that birnessite was reduced on the cathode and re-generated on the anode.

Fig. S10 shows the micromorphology of the iron-manganese nodule electrodes after five times of repeated adsorption. Without electrode polarity reversal, some cubic particles on the cathode and spindle-like crystals on the anode were observed, suggesting the formation of $CaCO_3$ and birnessite, respectively, as indicated by the XRD results (Figs. 4a and S9). With electrode polarity reversal, birnessite crystals were generated on both the cathode and anode, indicating a dissolution-recrystallisation process of birnessite. EDX was employed to evaluate the elemental composition and distribution on the iron-manganese nodule electrodes without electrode polarity reversal (Fig. 5 and Table S5).

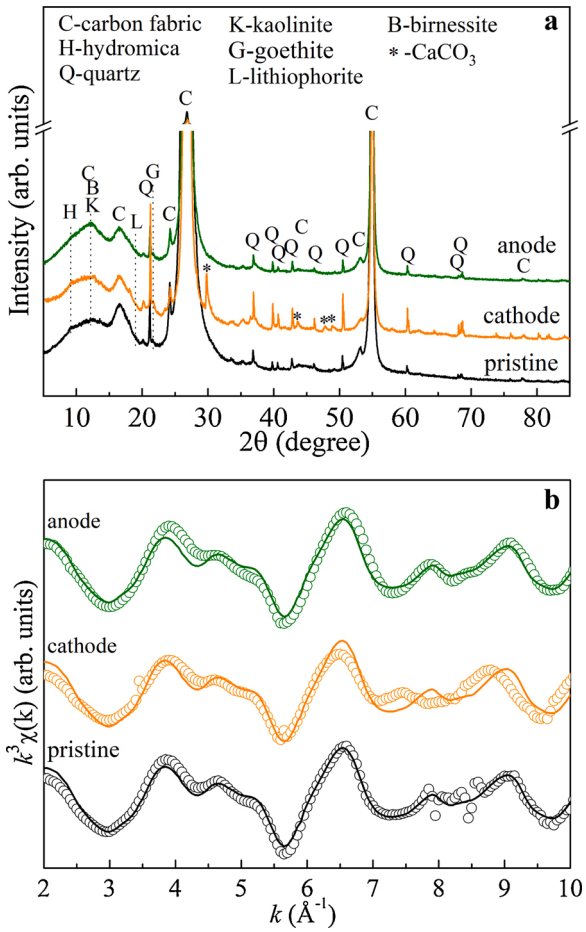

Fig. 4. XRD patterns (a) and Mn K-edge EXAFS spectra (the open circles are experimental curves and the solid lines are the best-fit linear combination) (b) of the pristine iron-manganese nodule electrode and the electrodes after five times of repeated adsorption in a symmetric electrode system without electrode polarity reversal at 1.2 V.

After five times of repeated adsorption, the molar ratio of Mn to Si in the area of lamellar structure on cathode surface (Area 2) decreased from 0.41 to 0.15; while that in the area of spindle-like crystals on anode surface (Area 4) increased to 1.21. The relative proportion of O also rose from 3.2% to 21.2% in Area 4, further demonstrating the dissolution-recrystallisation of birnessite. The relative proportions of Ca and O increased in the area of cubic particles on cathode surface (Area 3), which was in agreement with the XRD results (Figs. 4 and S9). The As was mainly adsorbed on manganese oxides in iron-manganese nodule electrode, as indicated by the EDX spectra.

The elemental valences and relative proportions in the electrodes after five times of repeated adsorption without electrode polarity reversal were analyzed using the As K-edge X-ray-absorption near-edge structure (XANES) and XPS spectra (Figs. 6 and 7). The positions of absorption edges in cathode and anode were close to those of Na_3AsO_4 in the XANES spectra, indicating that As exists primarily as As(V) in the cathode and anode (Fig. 6a). According to the XPS broad scans, the relative proportions of Mn, O and As in the pristine electrode were 1.05%, 26.83% and 0.07%, those in the cathode were 0.98%, 33.87% and 0.21%, and those in the anode were 11.64%, 42.78% and 0.23%, respectively (Fig. 6b and Table S6). In the Fe $2p_{3/2}$ spectra, the binding energy of 711.96 eV and the shape of Fe−O peak indicated that Fe was present as Fe(III) in the iron-manganese nodule electrodes (Fig. 6c) (Peng et al., 2017). In the As 3p and Si 2s spectra, the molar ratio of As to Si in the cathode and anode increased from 0.0073 to 0.11 and 0.33, respectively (Fig. 6d), further indicating the adsorption of As on both the cathode and anode.

The Mn $2p_{3/2}$ spectra were used to evaluate the relative proportion of Mn(II,III,IV) in the cathode and anode (Fig. 7a–c and Table S7). On the cathode, the relative proportion of Mn(IV) decreased from 46.1% to 32.3%; while that of Mn(III) and Mn(II) increased respectively from 42.8% and 11.1% to 47.3% and 20.4%; and the corresponding Mn average oxidation state (Mn AOS) decreased from 3.45 to 3.12. On the anode, the relative proportion of Mn(IV) increased to 66.5%; while that of Mn(III) and Mn(II) decreased respectively to 29.9% and 3.6%; and the corresponding Mn AOS increased to 3.63. In the O 1s spectra, the O in the form of O^{2-} increased from 4.6% to 7.4% and 50.7% in the cathode and anode, respectively (Fig. 7d and Table S8), which could be mainly ascribed to As adsorption, as well as the formation of $CaCO_3$ on the cathode and manganese oxides on the anode.

4. Discussion

4.1. As(III) oxidation

Arsenic was mainly present as As(V) on iron-manganese nodules (Fig. 6a), indicating the oxidation of As(III) during the electrochemical adsorption. The manganese oxides, especially birnessite, have strong adsorption capacity for As(III,V) and oxidation capacity for As(III). Almost all As was adsorbed as As(V) on the solid phase in the removal of As(III) or As(V) when using iron-manganese nodules or iron-manganese binary oxides (Chen et al., 2006; Zheng et al., 2020). As(III) can be adsorbed and oxidized by the Mn(IV) around the vacancy sites in birnessite (2Mn(IV) + As(III) → 2Mn(III) + As(V)), and the newly generated Mn(III) intermediates will also participate in As(III) oxidation (2Mn(III) + As(III) → 2Mn(II) + As(V)) (Gude et al., 2017). In this study, the high transformation efficiency from As(III) to As(V) achieved at open circuit also demonstrates the existence of chemical oxidation (Fig. 2a and b).

Besides chemical oxidation, As(III) can be directly electrochemically oxidized on the anode. As reported, about 50% of As(III) in the solution at an initial concentration of 75 mg L^{-1} can be oxidized to As(V) by the symmetric activated carbon electrodes at a constant cell voltage of 1.4 V (Dai et al., 2018). In this work, the anode potential reached about 0.75 V (*vs.* SCE) (Fig. S4), which was higher than the standard potential for the oxidation of H_3AsO_3 to H_3AsO_4 (0.28 V, *vs.* SCE) (Liu et al., 2019c), and thus facilitated As(III) oxidation on the anode.

Generation of H_2O_2 through the electrochemical reduction of dissolved O_2 on the cathode may also play a critical role in As(III) oxidation (Luong et al., 2018). The cathode potential (about −0.45 V, *vs.* SCE) at 1.2 V was remarkably lower than the standard potential for the generation of H_2O_2 from O_2 (0.029 V, *vs.* SCE), and H_2O_2 was indeed detected in this work (Fig. S11). In our previous work, the formation of H_2O_2 on birnessite cathode was found to contribute to As(III) oxidation (Liu et al., 2019c). According to the above analysis, the birnessite in iron-manganese nodules, the anode at high potential and the H_2O_2 formed on the cathode were involved in As(III) oxidation. Clarification of the contributions of these pathways to As(III) oxidation may help to understand the oxidation mechanism of As(III) by the symmetrical iron-manganese nodule electrodes. However, the capture of H_2O_2 is easily affected by the instability of superoxide enzyme under electrochemical reaction conditions, and it is difficult to quantitatively determine the ratio of As(III) oxidation through the direct electrochemistry reaction on the anode. Therefore, the relative contribution of each pathway to As(III) oxidation was not quantitatively characterized in this work.

4.2. As(V) removal

The total As removal efficiency was enhanced under the electrochemical reactions using symmetric iron-manganese nodule electrodes, and As(V) was detected in the cathode and anode. These results

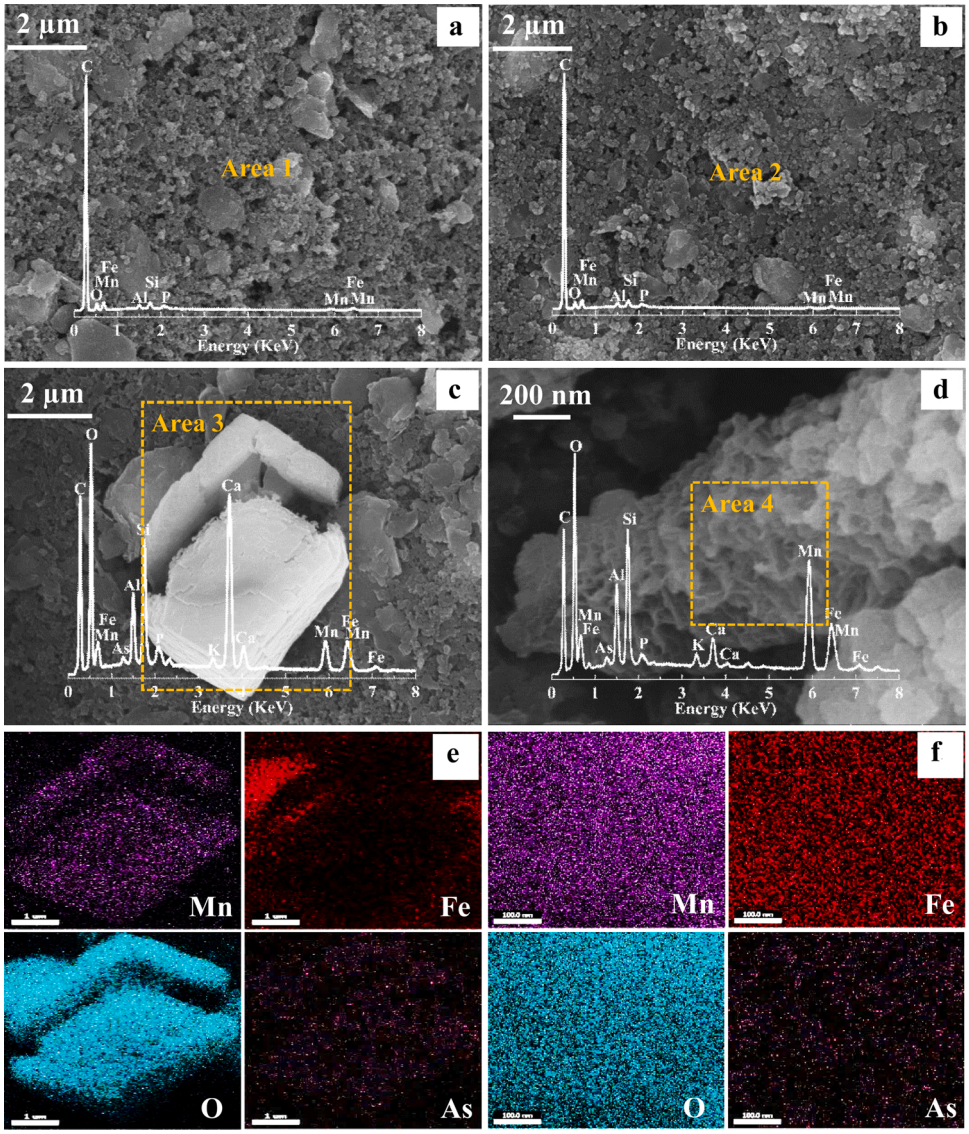

Fig. 5. SEM images and EDX analyses of the pristine iron-manganese nodules (a) and the cathode (b, c) and anode (d) after five times of repeated adsorption in a symmetric electrode system without electrode polarity reversal at 1.2 V and the corresponding EDX mappings for different elements in Area 3 (e) and Area 4 (f).

indicated that both electrochemical reduction on the cathode and electrochemical oxidation on the anode contribute to As adsorption.

About 67.1% of the removed total As was adsorbed on the cathode. Mn(IV) is more easily reduced than Fe(III), as indicated by the higher standard potential for the reduction of Mn(IV) to Mn(III) than that for the reduction of Fe(III) to Fe(II) (Marcus et al., 2004). In this work, reduction dissolution and phase transformation of iron oxides were not detected on the cathode (Figs. 4 and S9), and the Fe content in the cathode was close to that in the anode (Table S6), suggesting that the reduction of iron oxides in the cathode could be negligible. The relative proportions of Mn(II/III) and Mn(IV) increased and decreased, respectively, accompanied by a decrease of Mn AOS in the cathode (Table S7). Compared with lithiophorite, birnessite has higher adsorption and oxidation capacity, and thus can be more easily reduced (Kim et al., 2002), as indicated by the decrease in the relative proportion of birnessite and the increase in that of lithiophorite after electrochemical adsorption of As in this work (Table S4). When As(III) is oxidized by birnessite, the released Mn^{2+} will react with Mn(IV) at the edge of MnO_6 octahedral layer to produce Mn(III). Besides the vacancy sites, the newly formed Mn(III) can also act as additional adsorption sites for As(V) at the edge of $Mn(III)O_6$ octahedral layer (Lafferty et al., 2010). Therefore, the presence of Mn^{2+} can improve As(V) adsorption on some manganese oxides (Gude et al., 2017; Hou et al., 2017). In this work, total As removal efficiency was enhanced due to the formation of Mn(III) in iron-manganese nodules for the electrochemical reduction and adsorption of Mn^{2+} from wastewaters (Fig. S5).

At alkaline pH, during the adsorption of As(V) by iron-manganese oxides or biochar in the presence of Ca^{2+}, $CaHAsO_4$ and $Ca_3(AsO_4)_2$ precipitates are possibly formed due to the enrichment of As(V) on the surface of these adsorbents (Zhang et al., 2012; Chille et al., 2018; Zhong et al., 2020). In our previous work, the adsorption capacities of manganese oxides for Cu^{2+}, Cd^{2+} and Zn^{2+} were enhanced by adjustment of the chemical composition, crystal structure and surface charge under electrochemical reduction (Liu et al., 2018; Yang et al., 2018; Liu et al., 2019a). In this work, the electrochemical reduction of birnessite increased the adsorption capacity for Ca^{2+}, which induced the adsorption of CO_3^{2-} and As(V) on the iron-manganese nodule cathode (Fig. 4). After electrochemical adsorption using the synthesized iron-manganese oxide at 1.2 V for 24 h, the total As and As(III) concentrations respectively decreased to 21.0 and 2.1 μg L^{-1}, further indicating the promotion of As removal by Ca^{2+}. The chemical compositions of actual wastewaters are usually complicated, and some other coexisting ions may positively

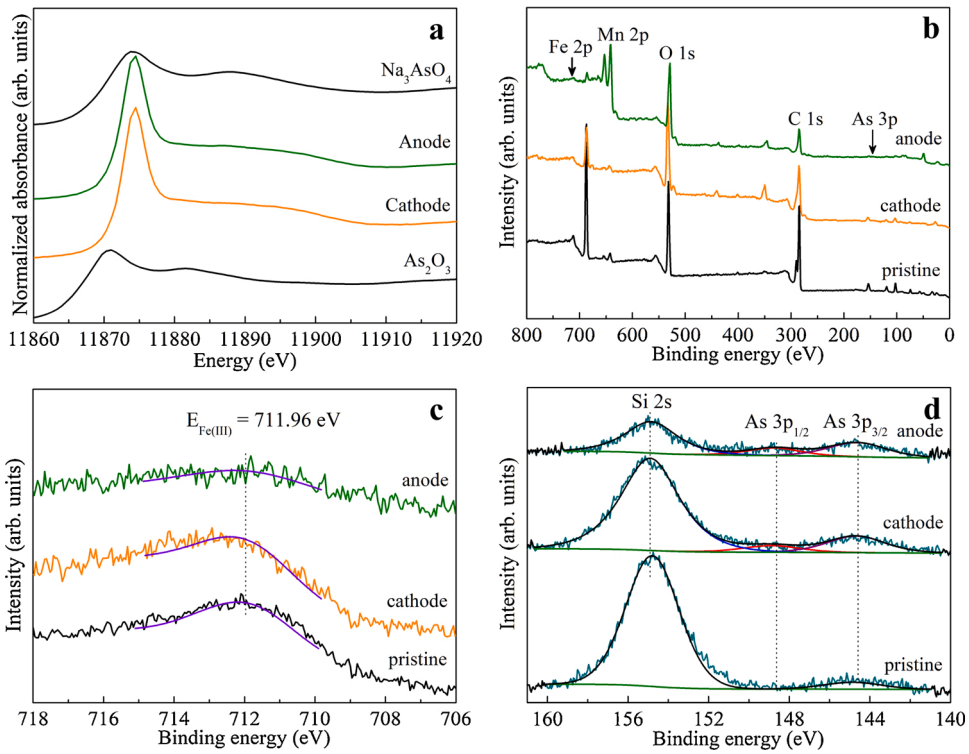

Fig. 6. As K-edge XANES (a), XPS broad scans (b), Fe 2p (c), As 3p and Si 2s (d) spectra of the pristine iron-manganese nodule electrode and the electrodes after five times of repeated adsorption in a symmetric electrode system at 1.2 V without electrode polarity reversal.

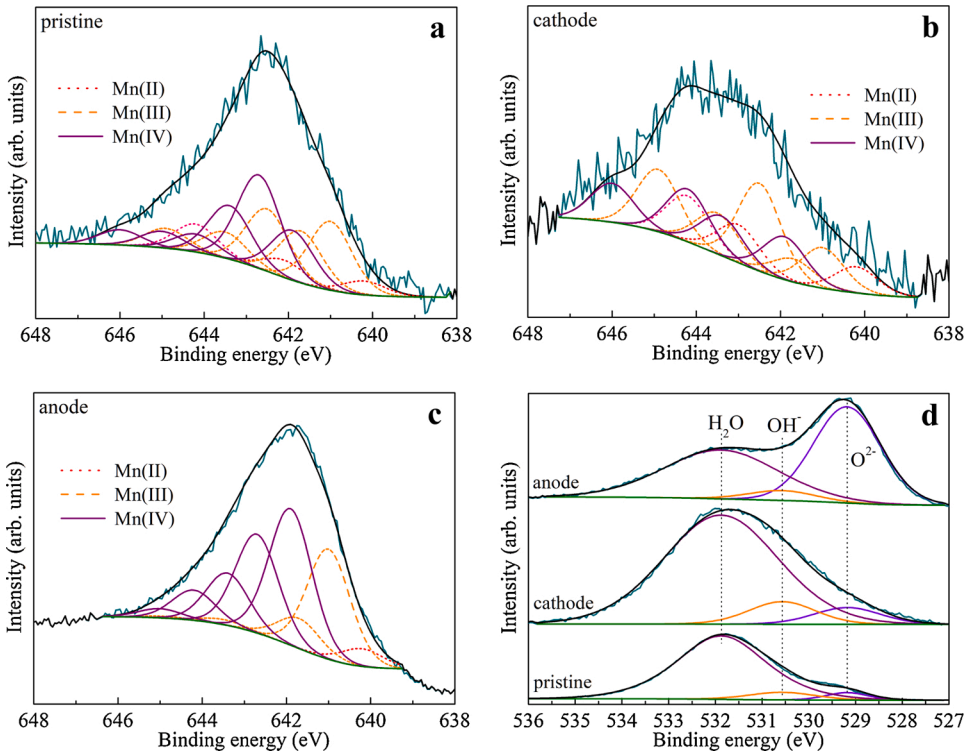

Fig. 7. Mn $2p_{3/2}$ (a–c) and O 1s (d) of the pristine iron-manganese nodules and the electrodes after five times of repeated adsorption in a symmetric electrode system at 1.2 V without electrode polarity reversal.

or negatively affect the electrochemical removal of As. For example, Mg^{2+} can also form complexes with As(V) (Chille et al., 2018), and PO_4^{3-} can compete with As(V) for adsorption sites on the surface of iron and manganese oxides (Deng et al., 2018). The effects of these coexisting ions on the electrochemical removal efficiency of As remain to be investigated in the future.

About 32.9% of the removed As was adsorbed on the iron-manganese nodule anode. An increase in positive charges on the anode surface can

promote As(V) adsorption (Dai et al., 2017). Generally, iron oxides have a higher adsorption isotherm capacity for As(V) than manganese oxides (Alvarez-Cruz and Garrido-Hoyos, 2019). However, the adsorption capacity and mechanism may be different under electrochemical redox. Our previous work has indicated that manganese oxides rather than iron oxides in iron-manganese nodule anode contribute much to As adsorption in the asymmetric electrode system with graphite paper as the cathode (Qiao et al., 2020). Fe(III) in the crystal of iron oxides with a high structure stability is difficult to be further oxidized, while Mn (II/III) in the manganese oxides can be electrochemically oxidized to Mn (IV), which increases the positive charges on the anode surface (Qiao et al., 2020). In this work, the relative proportions of Mn(IV) and Mn (II/III) also increased and decreased in the anode, respectively (Table S7). In addition, the released Mn^{2+} from the cathode can be re-oxidized on the anode. As reported, the birnessite passivation resulting from the reduction by released Mn^{2+} reduces As(III) oxidation ability (Lafferty et al., 2010; Gude et al., 2017). In this work, the re-oxidation of Mn^{2+} to birnessite effectively avoided the passivation process, which also provided more adsorption sites for As(V) on the anode.

4.3. Effect of cell voltage and reusability of the electrode

The As(III) oxidation efficiency and total As removal efficiency increased with increasing cell voltage. Cell voltage can affect the electrode potential and the redox of iron-manganese nodule electrode, affecting As(III) oxidation and total As removal. The cathode potential decreased from 0.2 V to −0.45 V (*vs.* SCE) with cell voltage increasing from 0 to 1.2 V (Fig. S4a), which promoted H_2O_2 formation and As(III) oxidation (Fig. S11). In addition, the adsorption of As(V) at the edge sites of MnO_6 octahedral layer was improved at a lower cathode potential and induced by the adsorbed Ca^{2+}. The further oxidation of more Mn(II/III) on the anode resulted in an increase in surface positive charge with increasing cell voltage (Fig. S4b), and the newly formed birnessite could provide more oxidation sites for As(III) and adsorption sites for As (V).

In the reuse of iron and manganese oxides, due to the formation of inner-sphere complexes during the adsorption, some complex regeneration operations are required and attenuation of As adsorption performance is inevitable (Dai et al., 2017; Chen et al., 2018). For example, during the electrochemical adsorption of As by the electrode composed of activated carbon and reduced graphene-iron composite, after electrochemical desorption with NaOH, a capacity retention rate of 80% was achieved at the second adsorption (Dai et al., 2017). In our previous work, the total As removal efficiency also decreased by 8.0% after five times of electrochemical adsorption using the synthesized birnessite (Liu et al., 2019c). In this work, the total As removal efficiency of the iron-manganese nodule electrode was only reduced by 2.9 % after five times of electrochemical adsorption. During the repeated electrochemical adsorption, As removal efficiency could be effectively improved by the polarity reversal of iron-manganese nodule electrode (Fig. 3). Our previous results have indicated that the dissolution-recrystallization process can fully expose the adsorption sites of the synthesized birnessite for heavy metal ions during the multi-cycle electrochemical redox reaction (Liu et al., 2018; Yang et al., 2018; Liu et al., 2019a). In this study, the dissolution-recrystallization process of iron-manganese nodules also occurred during the repeated adsorption with electrode polarity reversal (Figs. 5 and S10), which could improve the birnessite utilization ratio in the iron-manganese nodule electrode and promote the adsorption of As. The excellent reusability is supposed to greatly reduce the regeneration cost.

5. Conclusions

Electrochemically controlled redox of the manganese oxides in iron-manganese nodules was found to facilitate the detoxification of As in contaminated waters. The total As removal efficiency could reach 94.7% in a symmetric electrode system. Both the cathode and anode were demonstrated to play critical roles in As(III) oxidation and As(V) adsorption. Besides the chemical oxidation by the birnessite in iron-manganese nodules, As(III) was oxidized by the H_2O_2 formed at the cathode and electrochemically oxidized on the anode at high potential. On the cathode surface, the reduction of Mn(IV) to Mn(III) may provide additional adsorption sites for As(V), and promote As(V) adsorption induced by the simultaneously adsorbed Ca^{2+}. On the anode surface, Mn (II/III) oxidation could effectively avoid the passivation of birnessite resulting from the reduction by Mn^{2+}, which can facilitate As(III) oxidation and As(V) removal. The increase in anode potential and decrease in cathode potential accelerate the redox reaction with increasing cell voltage. The dissolution-recrystallization process of iron-manganese nodules facilitates the full exposure of the adsorption sites in birnessite for As during the repeated adsorption with electrode polarity reversal, which can greatly improve the birnessite utilization rate in the electrode and promote As adsorption. Overall, this study develops a new method for As detoxification in contaminated waters using natural iron-manganese nodules.

CRediT authorship contribution statement

Lihu Liu: Formal analysis, Writing - original draft, Investigation. **Qi Qiao:** Formal analysis, Writing - review & editing. **Wenfeng Tan:** Supervision. **Xuecheng Sun:** Supervision. **Chengshuai Liu:** Supervision. **Zhi Dang:** Supervision. **Guohong Qiu:** Supervision, Project administration, Conceptualization.

Declaration of Competing Interest

The authors declare that they have no known competing financial interests or personal relationships that could have appeared to influence the work reported in this paper.

Acknowledgements

Funding for this work came from the National Key Research and Development Program of China (Grant Nos. 2018YFD0800304 and2017YFD0801000), the National Natural Science Foundation of China (Grant Nos. 41571228, 41877025, 41877528 and 41425006), and the Fundamental Research Funds for the Central Universities(Grant Nos. 2662018JC055 and 2662017JC025). We thank Dr. Lirong Zheng and Dr. Shengqi Chu at Beijing Synchrotron Radiation Facility (BSRF) for assisting with XAS data collection, and Dr. Lihong Qin at Public Laboratory of Electron Microscope of Huazhong Agricultural University for helping with SEM characterization.

Appendix A. Supplementary data

Supplementary material related to this article can be found, in the online version, at doi:https://doi.org/10.1016/j.jhazmat.2020.123912.

References

Alvarez-Cruz, J.L., Garrido-Hoyos, S.E., 2019. Effect of the mole ratio of Mn/Fe composites on arsenic (V) adsorption. Sci. Total Environ. 668, 47–55.
Bai, Y., Yang, T., Liang, J., Qu, J., 2016. The role of biogenic Fe-Mn oxides formed in situ for arsenic oxidation and adsorption in aquatic ecosystems. Water Res. 98, 119–127.
Chen, Z., Kim, K.W., Zhu, Y.G., Mclaren, R., Liu, F., He, J.Z., 2006. Adsorption ($As^{III,V}$) and oxidation (As^{III}) of arsenic by pedogenic Fe–Mn nodules. Geoderma 136, 566–572.
Chen, J., Wang, J., Zhang, G., Wu, Q., Wang, D., 2018. Facile fabrication of nanostructured cerium-manganese binary oxide for enhanced arsenite removal from water. Chem. Eng. J. 334, 1518–1526.
Chille, D., Foti, C., Giuffre, O., 2018. Thermodynamic parameters for the protonation and the interaction of arsenate with Mg^{2+}, Ca^{2+} and Sr^{2+}: application to natural waters. Chemosphere 190, 72–79.

Dai, M., Zhang, M., Xia, L., Li, Y.M., Liu, Y.Y., Song, S.X., 2017. Combined electrosorption and chemisorption of As(V) in water by using Fe-rGO@AC electrode. ACS Sustain. Chem. Eng. 5, 6532–6538.
Dai, M., Xia, L., Song, S.X., Peng, C.S., Rangel-Mendez, J.R., Cruz-Gaona, R., 2018. Electrosorption of As(III) in aqueous solutions with activated carbon as the electrode. Appl. Surf. Sci. 434, 816–821.
Deng, Y., Li, Y., Li, X., Sun, Y., Ma, J., Lei, M., Weng, L., 2018. Influence of calcium and phosphate on pH dependency of arsenite and arsenate adsorption to goethite. Chemosphere 199, 617–624.
Eljamal, O., Mokete, R., Matsunaga, N., Sugihara, Y., 2018. Chemical pathways of Nanoscale Zero-Valent Iron (NZVI) during its transformation in aqueous solutions. J. Environ. Chem. Eng. 6, 6207–6220.
Garg, S., Rong, H., Miller, C.J., Waite, T.D., 2016. Oxidative dissolution of silver nanoparticles by chlorine: implications to silver nanoparticle fate and toxicity. Environ. Sci. Technol. 50, 3890–3896.
Gasparatos, D., 2013. Sequestration of heavy metals from soil with Fe-Mn concretions and nodules. Environ. Chem. Lett. 11, 1–9.
Gude, J., Rietveld, L., Van Halem, D., 2017. As(III) oxidation by MnO_2 during groundwater treatment. Water Res. 111, 41–51.
Guo, H., Ren, Y., Liu, Q., Zhao, K., Li, Y., 2013. Enhancement of arsenic adsorption during mineral transformation from siderite to goethite: mechanism and application. Environ. Sci. Technol. 47, 1009–1016.
Hou, J., Xiang, Y., Zheng, D., Li, Y., Xue, S., Wu, C., Hartley, W., Tan, W., 2017. Morphology-dependent enhancement of arsenite oxidation to arsenate on birnessite-type manganese oxide. Chem. Eng. J. 327, 235–243.
Kim, J.G., Dixon, J.B., Chusuei, C.C., Deng, Y.J., 2002. Oxidation of chromium(III) to (VI) by manganese oxides. Soil Sci. Soc. Am. J. 66, 306–315.
Lafferty, B.J., Ginder-Vogel, M., Zhu, M., Livi, K.J., Sparks, D.L., 2010. Arsenite oxidation by a poorly crystalline manganese-oxide. 2. Results from X-ray absorption spectroscopy and X-ray diffraction. Environ. Sci. Technol. 44, 8467–8472.
Lefkowitz, J.P., Elzinga, E.J., 2017. Structural alteration of hexagonal birnessite by aqueous Mn(II): impacts on Ni(II) sorption. Chem. Geol. 466, 524–532.
Liu, L., Luo, Y., Tan, W., Zhang, Y., Liu, F., Qiu, G., 2016. Facile synthesis of birnessite-type manganese oxide nanoparticles as supercapacitor electrode materials. J. Colloid Interface Sci. 482, 183–192.
Liu, L., Qiu, G., Suib, S.L., Liu, F., Zheng, L., Tan, W., Qin, L., 2017. Enhancement of Zn^{2+} and Ni^{2+} removal performance using a deionization pseudocapacitor with nanostructured birnessite and its carbon nanotube composite electrodes. Chem. Eng. J. 328, 464–473.
Liu, L., Tan, W., Suib, S.L., Qiu, G., Zheng, L., Huang, Q., Liu, C., 2018. Effective zinc adsorption driven by electrochemical redox reactions of birnessite nanosheets generated by solar photochemistry. ACS Sustain. Chem. Eng. 6, 13907–13914.
Liu, L., Peng, Q., Qiu, G., Zhu, J., Tan, W., Liu, C., Zheng, L., Dang, Z., 2019. Cd^{2+} adsorption performance of tunnel-structured manganese oxides driven by electrochemically controlled redox. Environ. Pollut. 244, 783–791.
Liu, L., Chen, H., Yang, X., Tan, W., Liu, C., Dang, Z., Qiu, G., 2019b. High-efficiency As (III) oxidation and electrocoagulation removal using hematite with a charge−discharge technique. Sci. Total Environ. 703, 135678.
Liu, L., Tan, W., Suib, S.L., Qiu, G., Zheng, L., Su, S., 2019c. Enhanced adsorption removal of arsenic from mining wastewater using birnessite under electrochemical redox reactions. Chem. Eng. J. 375, 122051.
Luong, V.T., Kurz, E.E.C., Hellriegel, U., Luu, T.L., Hoinkis, J., Bundschuh, J., 2018. Iron-based subsurface arsenic removal technologies by aeration: a review of the current state and future prospects. Water Res. 133, 110–122.
Marcus, M.A., Manceau, A., Kersten, M., 2004. Mn, Fe, Zn and As speciation in a fast-growing ferromanganese marine nodule. Geochim. Cosmochim. Acta 68, 3125–3136.
Mertens, J., Rose, J., Kagi, R., Chaurand, P., Plotze, M., Wehrli, B., Furrer, G., 2012. Adsorption of arsenic on polyaluminum granulate. Environ. Sci. Technol. 46, 7310–7317.
Ociński, D., Jacukowicz-Sobala, I., Mazur, P., Raczyk, J., Kociołek-Balawejder, E., 2016. Water treatment residuals containing iron and manganese oxides for arsenic removal from water – characterization of physicochemical properties and adsorption studies. Chem. Eng. J. 294, 210–221.
Peng, X., Xi, B., Zhao, Y., Shi, Q., Meng, X., Mao, X., Jiang, Y., Ma, Z., Tan, W., Liu, H., Gong, B., 2017. Effect of arsenic on the formation and adsorption property of ferric hydroxide precipitates in ZVI treatment. Environ. Sci. Technol. 51, 10100–10108.
Qiao, Q., Yang, X., Liu, L., Luo, Y., Tan, W., Liu, C., Dang, Z., Qiu, G., 2020. Electrochemical adsorption of cadmium and arsenic by natural Fe-Mn nodules. J. Hazard. Mater. 390, 122165.
Roychand, P., Marschner, P., 2013. Respiration in a sand amended with clay – effect of residue type and rate. Eur. J. Soil Biol. 58, 19–23.
Shan, C., Tong, M., 2013. Efficient removal of trace arsenite through oxidation and adsorption by magnetic nanoparticles modified with Fe–Mn binary oxide. Water Res. 47, 3411–3421.
Tang, W., He, D., Zhang, C., Kovalsky, P., Waite, T.D., 2017. Comparison of Faradaic reactions in capacitive deionization (CDI) and membrane capacitive deionization (MCDI) water treatment processes. Water Res. 120, 229–237.
Wei, Y., Wei, S., Liu, C., Chen, T., Tang, Y., Ma, J., Yin, K., Luo, S., 2019. Efficient removal of arsenic from groundwater using iron oxide nanoneedle array-decorated biochar fibers with high Fe utilization and fast adsorption kinetics. Water Res. 167, 115107.
Xu, J., Li, J., Wu, F., Zhang, Y., 2013. Rapid photooxidation of As(III) through surface complexation with nascent colloidal ferric hydroxide. Environ. Sci. Technol. 48, 272–278.
Yang, X., Liu, L., Tan, W., Qiu, G., Liu, F., 2018. High-performance Cu^{2+} adsorption of birnessite using electrochemically controlled redox reactions. J. Hazard. Mater. 354, 107–115.
Ying, S.C., Kocar, B.D., Fendorf, S., 2012. Oxidation and competitive retention of arsenic between iron- and manganese oxides. Geochim. Cosmochim. Acta 96, 294–303.
Zhang, G., Qu, J., Liu, H., Liu, R., Wu, R., 2007. Preparation and evaluation of a novel Fe-Mn binary oxide adsorbent for effective arsenite removal. Water Res. 41, 1921–1928.
Zhang, G., Liu, H., Qu, J., Jefferson, W., 2012. Arsenate uptake and arsenite simultaneous sorption and oxidation by Fe–Mn binary oxides: influence of Mn/Fe ratio, pH, Ca^{2+}, and humic acid. J. Colloid Interface Sci. 366, 141–146.
Zhang, G., Liu, F., Liu, H., Qu, J., Liu, R., 2014. Respective role of Fe and Mn oxide contents for arsenic sorption in iron and manganese binary oxide: an X-ray absorption spectroscopy investigation. Environ. Sci. Technol. 48, 10316–10322.
Zhao, S., González-Valle, Y.A., Elzinga, E.J., Saad, E.M., Tang, Y., 2018. Effect of Zn(II) coprecipitation on Mn(II)-induced reductive transformation of birnessite. Chem. Geol. 492, 12–19.
Zheng, Q., Hou, J., Hartley, W., Ren, L., Wang, M., Tu, S., Tan, W., 2020. As(III) adsorption on Fe-Mn binary oxides: are Fe and Mn oxides synergistic or antagonistic for arsenic removal? Chem. Eng. J. 389, 124470.
Zhong, D., Zhao, Z., Jiang, Y., Yang, X., Wang, L., Chen, J., Guan, C.Y., Zhang, Y., Tsang, D.C.W., Crittenden, J.C., 2020. Contrasting abiotic As(III) immobilization by undissolved and dissolved fractions of biochar in Ca^{2+}-rich groundwater under anoxic conditions. Water Res. 183, 116106.